Available online at www.sciencedirect.com
SCIENCE DIRECT®
Journal of Nuclear Materials 328 (2004) 137–145
journal of nuclear materials
www.elsevier.com/locate/jnucmat

Study of the β → α variant selection for a zircaloy-4 rod heated to the β transus in presence or not of an axial tensile stress

N. Gey [a,*], M. Humbert [a], E. Gautier [b], J.L. Béchade [c]

[a] Laboratoire d'Etude des Textures et Applications aux Matériaux LETAM, CNRS UMR 7078, ISGMP, Université de Metz, F-57045 Metz cedex 01, France
[b] Laboratoire de Science et Génie des Matériaux et de Métallurgie LSG2M, UMR 7584 CNRS/INPL, Ecole des Mines, Parc de Saurupt, F-54042 Nancy cedex, France
[c] CEA/DEN, Service de Recherches Metallurgiques Appliquées, CEA/Saclay, F-91191 Gif-sur-Yvette cedex, France

Received 12 June 2003; accepted 23 March 2004

Abstract

This contribution focuses on the β → α variant selection observed for a Zircaloy-4 rod, heated to the β transus, in presence (or not) of an axial tensile stress. The microstructures and the local textures of the α inherited phase have been characterized with crystal orientation maps. A specific processing of the data has been applied to distinguish on the maps, the colonies belonging to the same β grain and to deduce the parent grain orientations. The β grains were mainly oriented around the ⟨1 1 1⟩||AD fiber and had preferentially transformed into different α variants belonging to the ⟨1 1.0⟩||AD fiber. This variant selection is responsible for the sharp texture of the Zircaloy-4 rod after a treatment in the β field. Applying a stress at heating, reduces the β texture sharpness as well as the β → α variant selection. The origin of the variant selection mechanism is discussed and a variant selection model, based on the elastic anisotropy of the parent phase is applied to predict the variants favored by the transformation.

1. Introduction

Zircaloy-4 (Zy-4) is widely used as fuel cladding material for nuclear pressurized water reactors (PWR). In the event of a loss of coolant accident (LOCA), the temperature and the internal pressure of the cladding tubes rapidly increase and the Zy-4 material can undergo the α → β → α phase transformation in presence of stress [1,2]. The interaction between such a mechanical loading and the phase transformations strongly influences the resulting material behavior.

In previous works [3,4], this interaction has been investigated for various thermomechanical tests. In particular, an axial tensile stress was applied to a Zy-4 rod, during the α → β transformation, to study its effect on the material behavior. The subsequent β → α transformation at cooling was free of stress. The thermomechanical tests clearly pointed out the existence of transformation plasticity when the α → β transformation occurred under stress, as well as creep of the β phase. Some effects on the α inherited microstructures and textures have also been reported. In particular, the analysis of the α inherited textures showed a variant selection in the β → α phase transformation which decreases when stress were applied at heating.

In this contribution, this variant selection is analyzed considering local texture measurements. The α inherited microstructures were characterized with orientation

* Corresponding author. Fax: +33-3 87 31 53 77.
E-mail address: gey@letam.sciences.univmetz.fr (N. Gey).

0022-3115/$ - see front matter © 2004 Elsevier B.V. All rights reserved.
doi:10.1016/j.jnucmat.2004.03.003

maps obtained by electron back scattered diffraction (EBSD). Thanks to a specific processing of the orientation data, the variants formed in each parent β grain during the $\beta \rightarrow \alpha$ transformation have been identified and used to calculate the parent grain orientations. Therefrom the β texture can be evaluated and used to analyze the variant selection phenomenon.

2. Experimental procedure

2.1. Material and thermomechanical treatment

The material and the thermomechanical treatment have been detailed in [4]. The 6 mm diameter and 30 mm length samples were taken from the core of a Zy-4 rod. The axial direction (AD) of each sample corresponds to the AD of the rod. The heat treatment for a complete $\alpha \rightarrow \beta \rightarrow \alpha$ phase transformation sequence was carried out at 1000 °C in secondary vacuum, with heating and cooling rates of 10 °C/s.

In this investigation, two samples are considered. Sample A has been heat treated without applied stress. In the case of sample B, a controlled tensile stress of 8.2 MPa was applied parallel to AD during the heating step and removed after the temperature of 1000 °C was reached.

After the β treatment, both samples exhibit a classical microstructure inherited from the $\beta \rightarrow \alpha$ transformation and characterized by Widmanstätten α colonies.

2.2. Electron back scattered diffraction analysis

The EBSD technique was used to characterize the local texture inherited from the $\beta \rightarrow \alpha$ phase transformation. Orientation imaging of samples A and B was conducted fully automatically in a LEO 440 SEM equipped with the HKL EBSD software. For each sample, six EBSD maps covering each 900×750 μm were collected with a step size of 2.5 μm (corresponding to the size of a Widmanstätten lamella). In consequence, the orientations of a large number of colonies have been measured, even the colonies appearing very small on the observed surface. The α colonies can easily be distinguished on the orientation map as they correspond to domains characterized by more or less the same orientation. Of course, with the used step size, the lamella structure inside the α colonies is not revealed on the orientation map.

The resulting orientation data sets were processed according to the method proposed in [5]. First of all, specific α misorientation maps were built to systematically identify the α colonies inherited from the same parent β grain. Further, when at least 2 or 3 variants can be identified as inherited from the same a parent β grain, its orientation was determined as described in [5–7].

The orientations of the large number of α colonies observed were used to evaluate the orientation distribution function (ODF) of the α inherited phase. The ODF was calculated with a superposition of gaussian functions centered on each orientation. The latter was obtained by averaging all the measurements inside a colony. Each gaussian function was weighted by the volume fraction of the colony considered. One can remark that the texture of sample A and B had already been characterized in [4]. In this work, the orientations data had also been obtained using the EBSD technique. However, the experimental working conditions slightly differed. In [4], one used an automatic displacement of the stage and a large step size (without having for objective to build an orientation map) whereas in the present work, large orientation maps were acquired. It is to notice that both experimental working conditions lead to the same evaluation of the α inherited textures. This shows in both cases, the statistical reliability of the measured orientations.

3. Experimental results

The results of the EBSD analysis are given for sample A in Figs. 1 and 2, and for sample B in Figs. 3 and 4. Figs. 1 and 3 show for each sample, one of the six orientation maps acquired and the corresponding {0 0.2} and {1 1.0} pole projections. The α texture deduced from all the orientations measured, is represented by means of the {0 0.2} and {1 1.0} pole figures, respectively in Figs. 2 and 4, for sample A and B.

3.1. Textures of the α inherited phase

Both samples exhibit a nearly axisymmetric fiber texture around the rod axis. Two fiber components can be distinguished: a main $\langle 1\,1.0\rangle \| \mathrm{AD}$ fiber ($\vec{c}$ axes at 90° from AD) and a minor fiber component corresponding to the orientations of α crystallites having their $\vec{c}$ axes at about 30° from AD. It can be noticed that the α textures of both samples are similar in terms of orientation density localization. However, they show some differences in the texture sharpness and in terms of relative maximal density of each fiber. In fact, the maximum of the ODF has decreased from 12 (sample A) to 9 (sample B), whereas the texture index has decreased from 4 to 2.4. This mainly corresponds to a decrease of orientation density around the $\langle 1\,1.0\rangle \| \mathrm{AD}$ fiber, as seen in Figs. 1 and 3. The minor fiber component, corresponding to the orientations of α crystallites having their $\vec{c}$ axes at about 30° from AD, has an intensity of the same order for both samples (see the corresponding density levels in the pole figures).

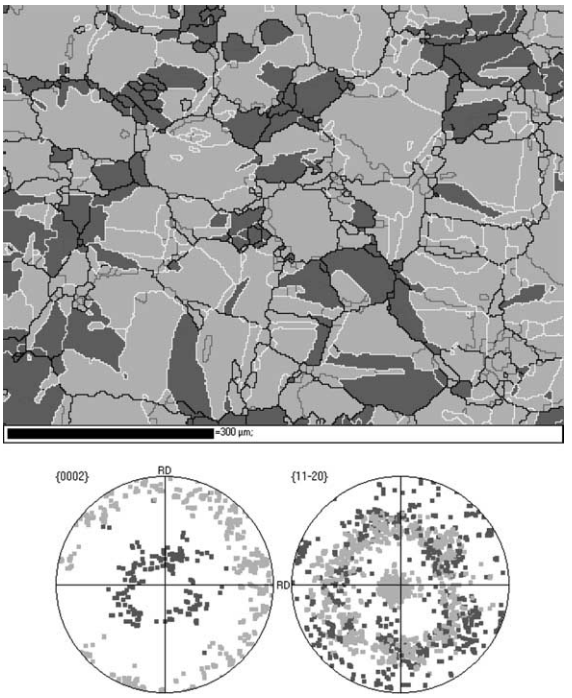

Fig. 1. Crystal orientation map of sample A and the corresponding {0 0.2}/{1 1.0} pole projections. The color of each pixel in the map is related to the measured orientation according to the color key given by the pole projections. The color key of the frontier lines between neighboring pixels allows to recognize α colonies inherited with a high probability from the same parent β grain (white lines) and the parent β grain boundaries (black and grey lines) – more details in the text.

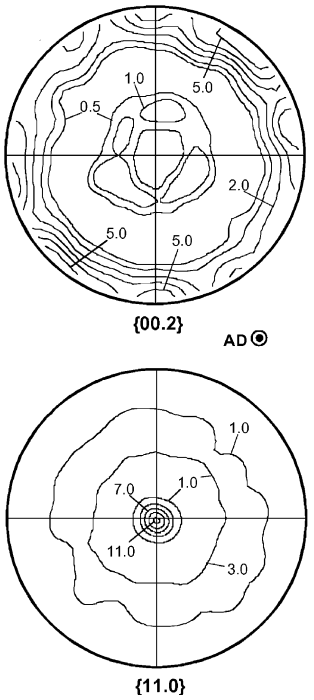

Fig. 2. {0 0.2} and {1 1.0} pole figures of the α inherited phase – sample A.

3.2. Orientation mapping of the α inherited phase

The maps shown in Figs. 1 and 3 contain information about the orientations of each measurement point and the misorientations between them. The color of each pixel in the map is related to the corresponding measured orientation, whereas the frontier lines between adjacent pixels reveal specific misorientation between them.

The pixels colored in light grey reveal the orientations belonging to the $\langle 1\,1.0\rangle \| \mathrm{AD}$ fiber ($\vec{c}$ axes at 90° from AD). Those colored in dark grey reveal the orientations belonging to the second fiber with the $\vec{c}$ axes at about 30° from AD (see the color key on the pole projection).

The color key of the frontier lines between pixels allows to distinguish the colonies inherited from the same β grain. In fact, a detailed analysis of the Burgers orientation relation shows that the α colonies related to the same parent grain are characterized by a limited number of misorientations between them. These misorientations, listed in Table 1, are used in Figs. 1 and 3 to recognize these coupled variants on the ESBP map. The white lines characterize the misorientations between adjacent pixels close to one of the theoretical misorientations given in Table 1 (with a tolerance of 5°). In this way, they exhibit adjacent colonies inherited with a high probability from the same parent. On the other hand, when the misorientation between adjacent pixels differs from those listed in Table 1, the corresponding colonies are obviously inherited from two different grains. These misorientations reveal the parent β grain boundaries. They are displayed by black and grey lines: The line is black when the corresponding misorientation angle is higher then 3° and grey when the corresponding misorientation angle is between 1° and 3°. Thus, the grey lines reveal α colonies being slightly misoriented and for which it is often difficult to know if they are inherited from the same parent grain or not. In this case, it is necessary to analyze the orientation of each colony with its neighborhood and find out with which neighboring β grain, its orientation is related.

The analysis of the α colonies inherited grain per grain shows that most of the parent β grains transform into several different variants, during the $\beta \rightarrow \alpha$ transformation. On the visible section of the β grains, one can often distinguish between 4 and 6 colonies characterized by different orientations. However, in each parent grain, the inherited colonies belong preferentially to the $\langle 1\,1.0\rangle \| \mathrm{AD}$ fiber. This trend clearly appears for both samples as seen

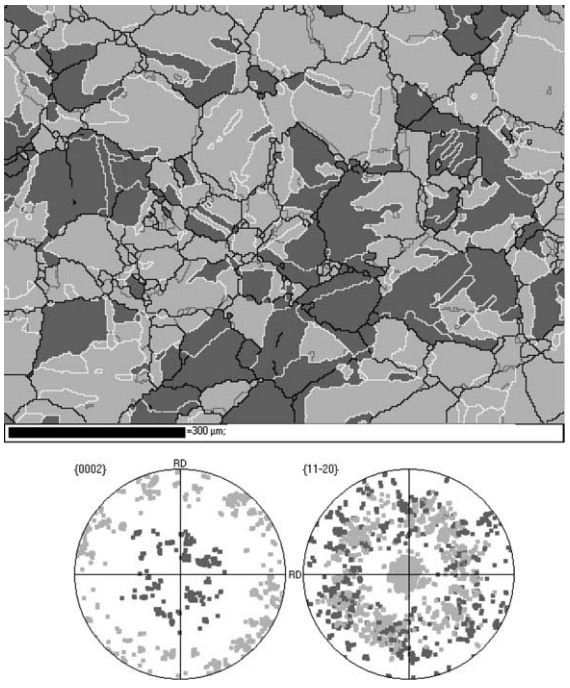

Fig. 3. Crystal orientation map of sample B and the corresponding {0 0.2}/{1 1.0} pole projections. The color of each pixel in the map is related to the measured orientation according to the color key given by the pole projections. The color key of the frontier lines between neighboring pixels allows to recognize α colonies inherited with a high probability from the same parent β grain (white lines) and the parent β grain boundaries (black and grey lines) – more details in the text.

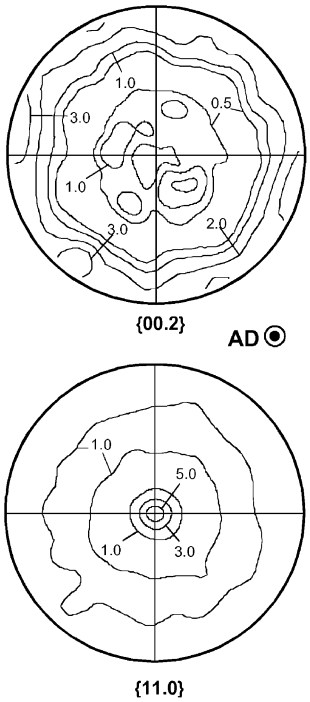

Fig. 4. {0 0.2} and {1 1.0} pole figures of the α inherited phase – sample B.

in Figs. 1 and 3. However, the proportion of variants belonging to this fiber differs. In fact, the analysis of all the acquired EBSD maps shows that for sample A, 75% of the α colonies were at 25° from the ⟨1 1.0⟩||AD fiber, whereas they were only 60% for sample B.

3.3. Evaluation of the β textures

The knowledge of the parent grain orientations is of importance to discuss the selective transformation of the α colonies belonging to the ⟨1 1.0⟩||AD fiber. As already discussed in [6,7], the orientation of a parent β grain can be deduced from correlations between the inherited variants. This kind of calculation has been applied to the EBSD data of samples A and B. Thanks to the specific maps given in Figs. 1 and 3, the colonies belonging to the same parent grain could be identified and used to calculate the parent orientation. For each sample, about 250 β orientations could be calculated and used to assess the parent textures.

Fig. 5 shows for each sample, the {1 0 0}/{1 1 1} pole figures calculated from these individual β orientations. The β textures are mainly characterized by strong densities around the ⟨1 1 1⟩||AD fiber. Few β grains belong to a minor ⟨1 0 0⟩||AD component. According to the statistical reliability of these orientations, it is difficult to discuss the texture more quantitatively. However, one notices that the β texture of sample B, heated under stress, is less sharp than that of sample A (as for the α texture inherited from the β → α transformation).

Table 1
Specific misorientations between α colonies inherited from a same β grain (*n* corresponds to one of the symmetrically equivalent rotation axe)

ω	$\vec{n}$
10°529	$\vec{c} = [0\,0.1]$
60°	$\vec{a}_2 = [\bar{1}\,2.0]$
60°832	$\vec{d}_1$ at 80°97 from $\vec{c}$ in $(\vec{d}_3, \vec{c})$ plane
63°262	$\vec{d}_2$ at 72°73 from $\vec{c}$ in $(\vec{a}_2, \vec{c})$ plane
90°	$\vec{d}_3$ at 5°26 from $\vec{a}_2$ in basal plane

These textures had also been evaluated in [4] from the global textures of the α inherited phase, thanks to a specific restitution method [8]. One has to remember that, in the case of variant selection in the β → α transformation, this method gives only qualitative information about the parent texture. However, the β textures calculated either with local correlations between α variants or with the global restitution method, show the same tendency.

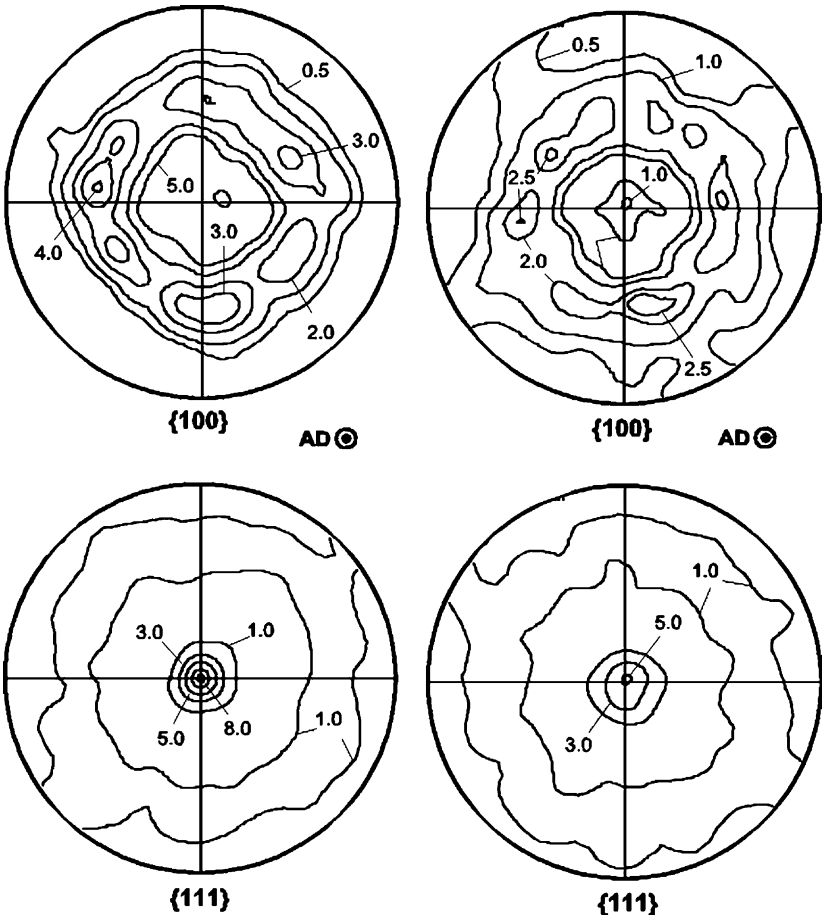

Fig. 5. {1 0 0} and {1 1 1} pole figures of the parent β phase for sample A and B.

3.4. Characterization of $\beta \rightarrow \alpha$ variant selection

To study the variant selection, it can be considered in a first approximation, that the β texture is mainly characterized by the ⟨1 1 1⟩||AD fiber. Any parent β grain belonging to this fiber, can give rise to 12 variants, according to the Burgers orientation relation. These variants can be arranged as follows:

Set 1: 6 α variants belonging to the ⟨1 1.0⟩||AD fiber.
Set 2: 6 α variants with the *c* axes at about 35° from AD.

An example is given in Fig. 6 for the parent β orientation characterized by (90°, 55°, 45°) Euler angles.

If no variant selection takes place during the transformation of such grains, one should observe 50% of α colonies belonging to set 1 and 50% to set 2. However, the EBSD maps of the α inherited phase clearly show that the variants of set 1 are favored during the $\beta \rightarrow \alpha$ transformation. Their volume fraction is of 75% for sample A and of 60% for sample B. This confirms that the sharp ⟨1 1.0⟩||AD fiber component of the α inherited texture is the result of a variant selection phenomenon. This variant selection is relatively sharp when no stress is applied. Applying a tensile stress at heating reduces the sharpness of the β texture as well as the variant selection at cooling.

4. Discussion of the variant selection mechanism

4.1. Thermodynamic aspects of the transformation

In the analyzed case, phase transformation occurs under similar conditions i.e. same cooling law and no applied stress. Therefore the free energy variation due the nucleation of an α grain within the β phase comprises three main contributions:

- A volume free energy reduction $V\Delta g^{\text{chem}}_{\beta-\alpha}$ related to the creation of an α inclusion Ω of volume V; $\Delta g^{\text{chem}}_{\beta-\alpha}$ is the chemical free energy (Gibbs energy)

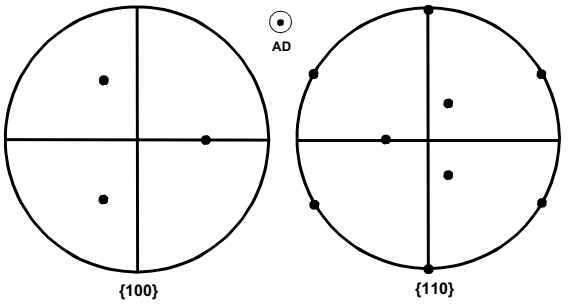

(a) specific parent β orientation belonging to the <111>//AD fibre

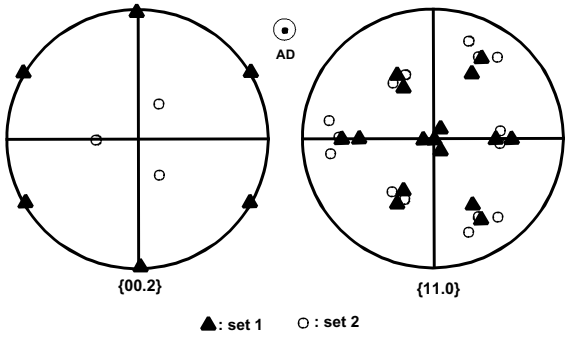

(b) corresponding inherited α orientations

Fig. 6. Characteristic pole projection of the potential variants inherited from the β orientation characterized by (90°, 55°, 45°) Euler angles.

variation associated with the transformation from β to α per unit volume.

- A free energy increase $S\Delta g^{\text{int}}_{\beta-\alpha}$ due to the creation of an interface S between the α inclusion Ω and the β matrix. $\Delta g^{\text{int}}_{\beta-\alpha}$ is the interface energy per unit area.
- A positive misfit strain energy $\Delta g^{\text{def}}_{\beta-\alpha}$ per unit volume of the α phase due to the fact that the transformed volume does not perfectly match the initial volume occupied by the matrix. This term is often estimated using Eshelby's inclusion approach, therefore its value is dependent on the volume of the nucleus.

This leads to the total free energy change:

$$\Delta G_{\beta-\alpha} = V\Delta g^{\text{chem}}_{\beta-\alpha} + S\Delta g^{\text{int}}_{\beta-\alpha} + V\Delta g^{\text{def}}_{\beta-\alpha}. \quad (1)$$

The morphology and orientation of the new phase is resulting from this global balance. Some preferential orientation can be associated with anisotropy in the interface energy, or anisotropy in the misfit strain energy. In the following, we were particularly interested by the role of the misfit strain energy $\Delta g^{\text{def}}_{\beta-\alpha}$ which varies according to the selected variant in the transformation. In fact, the nucleation of a given variant implies a specific transformation strain ε^{tr} leading to an increase of the elastic strain energy. The strain energy for each α variant depends on its orientation and the elastic behavior of the new phase as well as the one of the parent phase. Moreover any anisotropy in the elastic behavior of the new or the parent phase will lead to changes in the elastic strain energy.

Due to the symmetry of the parent phase, a restricted number of 12 differently oriented α nuclei (variant) can develop within a single β crystal. Thus, a specific positive misfit strain energy $\Delta g^{\text{def}}_{\beta-\alpha}$ corresponds to each of these 12 nuclei. As physically the transformation takes place providing that it reduces the maximum the total free energy of the system, it can be assumed that the variants which are preferentially selected in the transformation process, are those associated with the smallest positive misfit strain energy $\Delta g^{\text{def}}_{\beta-\alpha}$. This means that the surface energy is taken as constant for all cases.

4.2. Calculation of the misfit elastic strain energy related to a variant

The calculation of the misfit elastic strain energy has been performed owing to the well known 'equivalent inclusion method' due to Mura [9]. Application of this method to phase transformation was exposed in a previous paper [10].

By using the concept of eigenstrain, the method simulates the stress and the stress disturbance caused by an inclusion Ω of elastic constants C^*_{ijkl} (inhomogeneous inclusion) within an infinite matrix of elastic constants C_{ijkl}. The inclusion Ω of elastic constants C^*_{ijkl} is substituted by an inclusion Ω of the same elastic constants C_{ijkl} as the matrix with an eigenstrain ε^*_{mn} which causes the equivalent stress disturbance (due to the difference in elastic behavior between the matrix and the inclusion). The eigenstrain ε^*_{mn} is chosen so as to satisfy the following relation (Relation 22.13.11 of Ref. [9]):

$$\begin{aligned}\sigma^*_{ij} &= C^*_{ijkl}(S_{klmn}(\varepsilon^*_{mn} + \varepsilon^{\text{tr}}_{mn}) - \varepsilon^{\text{tr}}_{kl}) \\ &= C_{ijkl}\big(S_{klmn}(\varepsilon^*_{mn} + \varepsilon^{\text{tr}}_{mn}) - (\varepsilon^*_{kl} + \varepsilon^{\text{tr}}_{kl})\big),\end{aligned} \quad (2)$$

where σ^*_{ij} is the homogeneous internal stress in the inclusion and $\varepsilon^{\text{tr}}_{ij}$ is the transformation strain. The quantities S_{klmn}, characterizing the Eshelby tensor are shape dependent. They require the calculation of Green's functions and were calculated according to [9]. ε^*_{mn} is deduced from the right sides of relation (2). The stress σ^*_{ij} can then be calculated as well as the misfit elastic strain energy density $\Delta g^{\text{def}}_{\beta-\alpha}$ noted for a sake of simplicity w^*:

$$w^* = -\frac{1}{2}\sigma^*_{ij}\cdot\varepsilon^{\text{tr}}_{ij}. \quad (3)$$

Thus, the elastic strain energy density required for the nucleation of a variant, oriented $\Delta g_0 S_p \cdot g$, reads:

$$w^*(S_p \cdot g) = -\frac{1}{2}\sigma^*_{ij}(S_p \cdot g) \cdot \varepsilon^{tr}_{ij}(S_p \cdot g). \quad (4)$$

In this relation, $\sigma^*_{ij}(S_p \cdot g)$ (resp. $\varepsilon^{tr}_{ij}(S_p \cdot g)$) expresses the stress components in the medium reference frame (resp. the transformation strain tensor) of the pth variant nucleus for a β grain in orientation g. S_p is one among the 24 rotations of the BCC symmetry group. In fact, due to specificity of the Burgers orientation relation Δg_0, only 12 rotations of the BCC symmetry group are necessary to define the 12 differently oriented variants. Thus p runs from 1 to 12.

4.3. Model of the variant selection

The variant selection is assumed to be linked to the elastic strain energy. Among all the potential variants which can be inherited from a given β parent grain, only those for which the elastic strain energies are the lowest, are selected.

For a parent crystal in orientation g, the 12 elastic strain energy densities $w^*(S_p \cdot g)$ $(p = 1, 2, \ldots, 12)$ corresponding to the 12 variants are calculated using Eq. (4).

The elastic constants of the medium C_{ijkl} are assumed to be equal to those of the polycrystal. Because the transformation starts at a great number of locations dispersed in the material and whose orientations are different, it is reasonable to think that in mean, the elastic reaction of the material to the transformation strain of variants with the same orientation, can be calculated from the effective elastic behavior of the sample. This will also integrate the interaction of the nucleus which forms near the β/β grain boundary, rather to consider the elastic behavior of the single β grain. The effective elastic constants of the polycrystal C_{ijkl} are generally well represented by the Hill elastic constants C^{Hill}_{ijkl} calculated as in [12] from the texture and from the elastic single crystal constants of BCC Zr at 1200 °K [13] ($C^{\beta}_{1111} = 1.08$, $C^{\beta}_{1122} = 0.93$, $C^{\beta}_{1212} = 0.38$ in 10^5 MPa).

The transformation strain $\varepsilon^{tr}_{ij}(S_p \cdot g)$ is replaced by the homogeneous lattice strain $\varepsilon^{B}_{ij}(S_p \cdot g)$ (Bain strain in steels) as justified in [11] for Zr transformation. The lattice transformation strain ε^{B}_{ij} which transforms the BCC cubic cell to an HCP cell, according to the Burgers orientation relation reads in the BCC reference frame $\left\{X = \left[\frac{1}{\sqrt{2}}; \frac{1}{\sqrt{2}}; 0\right], Y = \left[\frac{\bar{1}}{\sqrt{2}}; \frac{1}{\sqrt{2}}; 0\right], Z = [0; 0; 1]\right\}$:

$$[\varepsilon^{B}_{ij}] = \begin{bmatrix} \frac{c_\alpha}{a_\beta\sqrt{2}} - 1 & & \\ & \frac{\sqrt{3}\cdot a_\alpha}{\sqrt{2}\cdot a_\beta} - 1 & \\ & & \frac{a_\alpha}{a_\beta} - 1 \end{bmatrix} = \begin{bmatrix} -0.1 & & \\ & 0.1 & \\ & & 0.0 \end{bmatrix} \quad (5)$$

with the cell parameters of Zr ($a_\beta = 3.609$ Å, $a_\alpha = 3.248$ Å, $c_\alpha = 5.198$ Å).

In order to make the calculations easier, nuclei Ω were assumed as spherical. Moreover the calculations were performed considering the elastic constants of the nuclei C^*_{ijkl} to be equal to the elastic constants C^{β}_{ijkl} of parent phase (resp. C^{α}_{ijkl} of the inherited phase). The simulation results, the closest to the experimental observations and given in the next section, corresponded to the use of C^{β}_{ijkl}. This would substantiate the fact that the variant selection is related to the early stage of the transformation, when the material is, still for a short time, in BCC phase.

4.4. α Textures simulated with variant selection

Fig. 7 illustrates the elastic anisotropy (in the β phase) of samples A and B by the Young modulus in the plane (AD–RD) calculated from the Hill elastic constants C^{Hill}_{ijkl}. The variations for sample B is less important than for sample A. The difference of elastic anisotropy between sample A and B could explain the difference in variant selection severity.

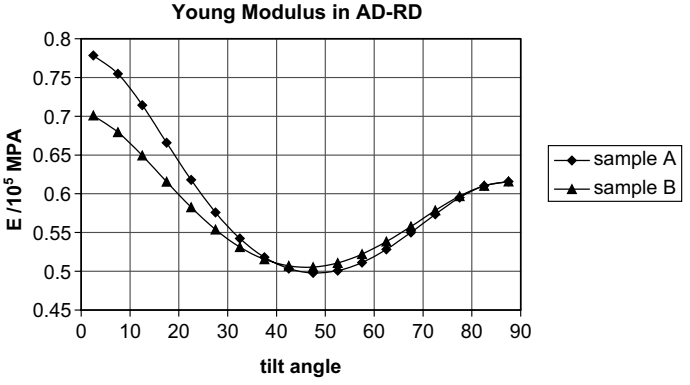

Fig. 7. Anisotropy of the Young modulus in the plane AD–RD for samples A and B.

As a matter of fact, Fig. 8 displays the elastic strain energy densities of all the 12 variants for samples A and B. One observes that it is comprised between 150.5 and 153.4 MJ/m^3 for sample A with some differences according to the variants. For sample B, the spread is less important (between 150.8 and 152.7 MJ/m^3) and more homogeneous whatever the variant.

In this paper, we considered that the selected variants are those for which the elastic strain energy density is less than a threshold of 152.0 MJ/m^3. The orientation of

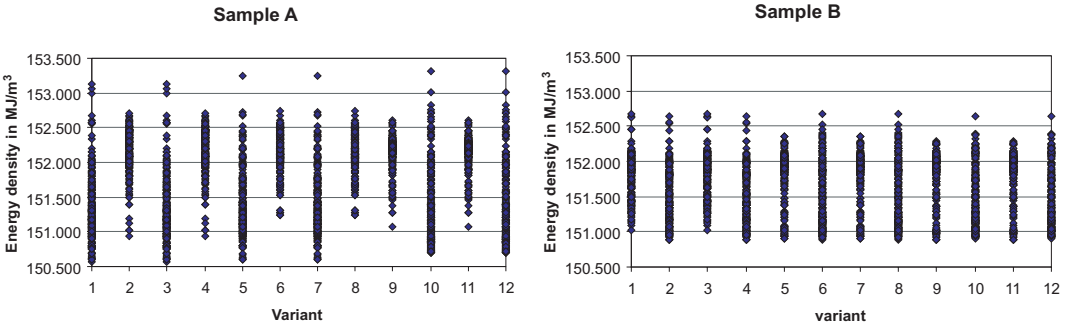

Fig. 8. Elastic strain energy densities of the 12 variants of each orientation in samples A and B.

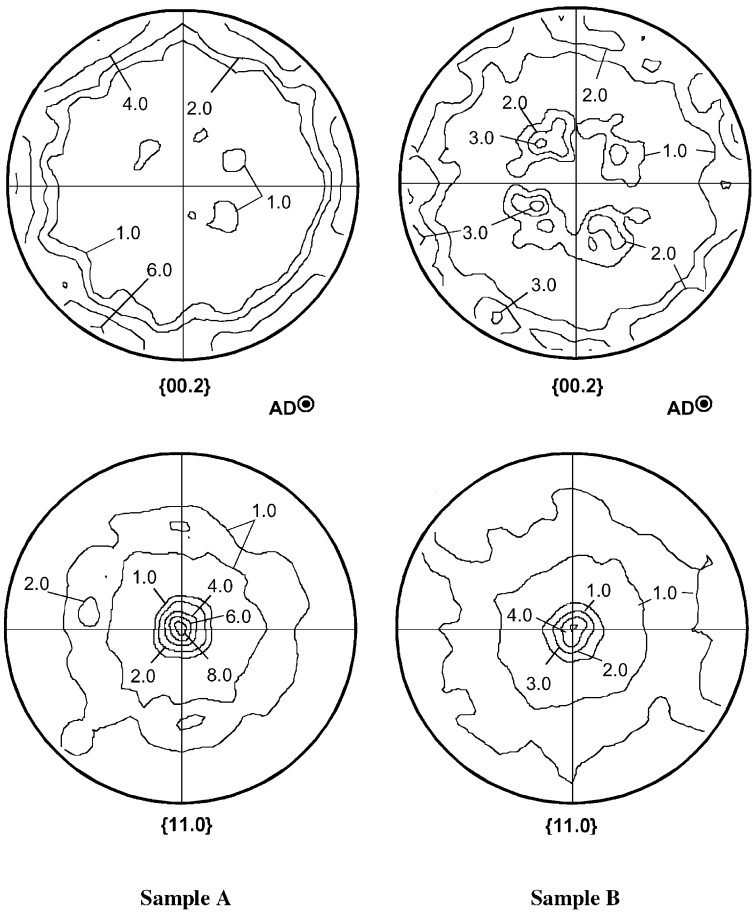

Fig. 9. {0 0.2} and {1 1.0} pole figures calculated with variant selection for sample A and sample B.

one selected variant is $\Delta g_0 S_p.g$ and its weight is equal to $V_1(g)/N_v$ where $V_1(g) = f_1(g) \times \Delta g$ is the parent β crystal volume in orientation g and N_v the number of variants, selected according to the threshold value. Fig. 9 shows the calculated {0 0 0.2} and {1 1 0} pole figures corresponding to sample A and sample B. The comparison between the experimental pole figures (Figs. 2 and 4) shows that the simulation of the variant selection respects the general trends for both samples with a stronger selection for sample A.

These results could be interpreted as follows:

Without an applied stress at heating, the β matrix presents a relatively strong texture and its resulting elastic anisotropy allows specific α variants to nucleate preferentially on cooling, imposing the lowest strain energy increase to the polycrystal. With an applied stress on heating, the β texture is smoother and its elastic anisotropy is reduced. Because the elastic behavior is less anisotropic in this last case, the variant selection during the $\beta \rightarrow \alpha$ transformation is less effective for similar cooling conditions.

5. Conclusion

The α inherited microstructure and local texture of a Zy-4 rod, heated to the β transus, in presence (or not) of an axial tensile stress, was characterized with specific crystal orientation maps. Without applied stress, the inherited texture shows strong densities around the $\langle 1\,1\,0\rangle \| \mathrm{AD}$ fiber and a minor fiber component with the $\vec{c}$ axes at 35° from AD. Applying a stress up to 8.8 MPa at heating, reduces the texture sharpness.

A specific processing of the α crystal orientation maps was applied to distinguish on the maps, the colonies belonging to the same β grain and deduce from their orientations, the parent grain orientations. This information was useful to study the $\beta \rightarrow \alpha$ variant selection. In fact, it clearly appears that the β grains were mainly oriented around the $\langle 1\,1\,1\rangle \| \mathrm{AD}$ fiber and had preferentially transformed into different variants belonging each to the $\langle 1\,1\,0\rangle \| \mathrm{AD}$ fiber. The calculation of the potential variants growing from such β grains shows that without variant selection, one should observe 50% of α colonies belonging to the $\langle 1\,1\,0\rangle \| \mathrm{AD}$ fiber and 50% to a fiber component with the $\vec{c}$ axes at 35° from AD. The difference between this simulation and the experimental observations reveals a variant selection mechanism. Applying a stress at heating, reduces the β texture sharpness as well as the $\beta \rightarrow \alpha$ variant selection.

The origin of the variant selection mechanism was finally discussed and assumed to be related to the elastic anisotropy of the β matrix. A variant selection model was proposed in which the favored variants are those imposing the lower elastic strain energy to the polycrystal. Applied to a β grain orientation belonging to the $\langle 1\,1\,1\rangle \| \mathrm{AD}$ fiber, the model allows to predict the variants favored by the transformation.

References

[1] C. Lemaignan, A.T. Motta, in: R.W. Cahn et al. (Eds.), Nuclear Materials II, Materials Science and Technology, vol. 10B, VCH, 1994, p. 1.
[2] F.J. Erbacher, S. Leistikow, in: R.B Adamson, L.F.P. Van Swam (Eds.), Zirconium In the Nuclear industry: 7th International Symposium, ASTM STP 939, American Society for Testing Materials, Philadelphia, 1987, p. 451.
[3] S. Fréchinet, PhD thesis, Ecole des Mines de Paris, 2001.
[4] N. Gey, E. Gautier, M. Humbert, A. Cerqueira, J.L. Béchade, P. Archambault, J. Nucl. Mater. 302 (2002) 175.
[5] N. Gey, M. Humbert, J. Mater. Sci. 38 (2003) 1289.
[6] M. Humbert, H. Moustahfid, F. Wagner, C. Esling, Scri. Metall. Mater. 30 (1994) 377.
[7] M. Humbert, N. Gey, J. Appl. Crystallogr. 35 (2002) 401.
[8] M. Humbert, N. Gey, C. Esling, J. Appl. Crystallogr. 33 (2000) 206.
[9] T. Mura, Micromechanics of Defects in Solids, Kluwer, Dochdrecht, 1991.
[10] M. Humbert, N. Gey, Acta Mater. 51 (2003) 4783.
[11] A. Kelly, G.W. Groves, Crystallography and Crystal Defects, Longman, London, 1970.
[12] H.J. Bunge, Texture Analysis in Materials Science, Butterworths, London, 1982.
[13] A. Heiming, W. Petry, J. Trampenau, M. Alba, C. Herzig, H.R. Schober, G. Vogl, Phys. Rev. B 43 (1991) 10948.